Spurious Fields in Time Domain Computations of Scattering Problems*

Urve Kangro and Roy Nicolaides
Department of Mathematics
Carnegie-Mellon University
Pittsburgh, PA 15213

Abstract

In this paper two-dimensional electromagnetic scattering problems with a time-periodic incident field are considered. The scatterer is a perfect conductor, and an artificial boundary condition is used. The large time behavior of solutions, depending on (divergence-free) initial conditions, is characterized. It turns out that in addition to the expected time-periodic solution the limiting solution may also contain a spurious stationary field. The source of the stationary field is explained and equations describing it are obtained. Several avoidance strategies are discussed, and numerical comparisons of these techiques are given.

*This work was supported by the United States Air Force Office of Scientific Research under grant F-49620-94-1-0311. Research was also supported by the National Aeronautics and Space Administration under NASA Contract No. NAS1-19480 while the authors were in residence at the Institute for Computer Applications in Science and Engineering (ICASE), NASA Langley Research Center, Hampton, VA 23681-0001.

1. INTRODUCTION

For solving scattering problems with a time-periodic incident field, the periodic solution is often obtained by choosing initial conditions and time marching Maxwell's curl equations to a periodic state. The initial conditions must satisfy the divergence equations but are otherwise arbitrary.

When this time marching method is used to solve scattering problems for perfect conductors it is found that the computed periodic solutions are "contaminated" by spurious stationary components. For example, in two dimensional transverse magnetic calculations it is observed that the magnetic field is affected by a spurious component; in three dimensions both the magnetic and electric fields are affected. The spurious fields can be relatively large and must usually be removed empirically by postprocessing, for example by peak-to-peak averaging [2], [3], or by the postprocessing method mentioned in section 4 below. These methods are usually effective and permit quantities such as radar cross sections to be obtained from the resulting numerical data. However, postprocessing introduces additional uncertainties and it is worthwhile to try to obtain accurate numerical solutions directly.

In this paper we will explain the origin of the spurious fields and obtain the differential equations and boundary conditions which characterize them. Based on these results we will propose some techniques which enable accurate results to be found directly and efficiently without postprocessing. We will provide numerical comparisons of the techniques.

The next section illustrates the occurrence of a spurious field in the relatively simple setting of a two dimensional transverse magnetic computation. Then we explain the source of this field and derive the equations which define it. Following that we discuss some avoidance strategies and illustrate their properties. The remainder of the paper extends the results to other problems and briefly mentions some mathematical issues which are analysed in detail in [4].

2. THE MAGNETIC OFFSET

In a two dimensional transverse magnetic problem it is the magnetic field which is affected by the spurious stationary component. To illustrate the spurious field we consider the following transverse magnetic scattering problem: in Ω,

$$\epsilon \frac{\partial \mathbf{E}}{\partial t} = \mathbf{curl}\,\mathbf{H} \tag{1}$$

$$\mu \frac{\partial \mathbf{H}}{\partial t} = -\mathbf{curl}\,\mathbf{E} \tag{2}$$

$$\mathrm{div}\,\mathbf{H} = 0 \tag{3}$$

with boundary conditions

$$\mathbf{E} = -\mathbf{E}_i \qquad \text{on } \Gamma_s \tag{4}$$

$$\mathbf{E} - c\mu\mathbf{H} \times \mathbf{n} = 0 \qquad \text{on } \Gamma_o \tag{5}$$

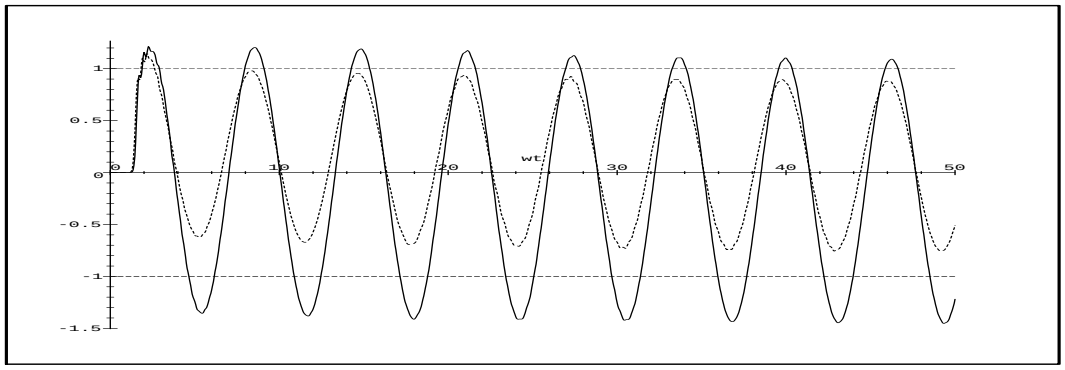

Figure 1: The time history of $\mathbf{H}_x$ (solid line) and $\mathbf{H}_y$ (dashed line).

and initial conditions

$$\mathbf{E}(\mathbf{x},0) = \mathbf{E}_0(\mathbf{x}), \qquad \mathbf{H}(\mathbf{x},0) = \mathbf{H}_0(\mathbf{x}). \tag{6}$$

In these equations, $\mathbf{E}$ and $\mathbf{H}$ denote the scattered field variables, $\mathbf{E}_i$ is the incident field, Γ_s denotes the boundary of the (perfect conductor) scatterer and Γ_o is the artificial outer boundary. Ω denotes the domain between the inner and outer boundaries, $\mathbf{n}$ is the outer normal to Ω and $\mathbf{x} = (x, y)$. We assume that $\mathbf{E}_i$ can be written in the form

$$\mathbf{E}_i(\mathbf{x}, t) = e^{i\omega t}\widetilde{\mathbf{E}}_i(\mathbf{x}),$$

and we look for the time-periodic solutions of (1)–(6) in a similar form. For simplicity, we are assuming a first order radiation condition on the outer boundary . The results are not materially affected if higher order radiation conditions are used.

To illustrate the magnetic offset we take a square scatterer with sides aligned with the coordinate axes and electric size 1 based on half the side length of the square. The scatterer is illuminated from the $(1, 0)$ direction by a field of the form $1000e^{i(\omega t - \mathbf{k}\cdot\mathbf{x})}$. The outer boundary is $\frac{4.5}{\pi}$ wavelengths (4.5 body lengths) from the center of the scatterer. This problem was marched to a periodic state, starting from zero initial conditions, using the standard uniform mesh "FDTD" scheme [1] with 20π points per wavelength and with a timestep of $1/\sqrt{2}$ the maximum size allowed by the stability condition.

In Figure 1 we show a time history of $\mathbf{H}_x$ and $\mathbf{H}_y$ sampled at the points $(-\frac{1}{\pi}, \frac{20.5}{20\pi})$ and $(-\frac{19.5}{20\pi}, \frac{1}{\pi})$, respectively (measured from the center of the body in wavelengths). While the records appear to approach periodic functions, they are not symmetric about the horizontal axis and consequently they cannot be of the desired form $e^{i\omega t}\mathbf{H}(\mathbf{x})$. A similar situation holds at the other mesh points, the amount of the offset being a function of position. This function is spurious and is not part of the solution to the periodically forced scattering problem. We wish to characterize it with a view to eliminating it altogether.

In contrast to Figure 1, Figure 2 shows the time history of the electric field at the point $(-\frac{1}{\pi}, \frac{1}{\pi})$. There is no obvious problem with this solution and in fact it is close to the exact

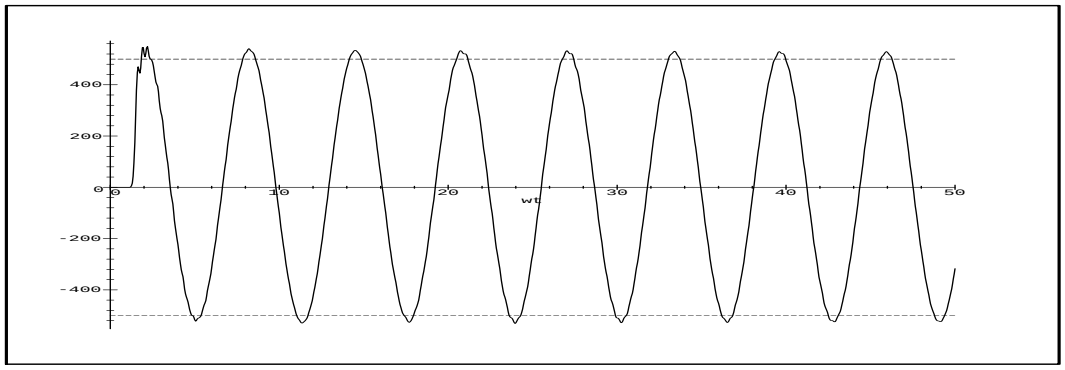

Figure 2: The time history of $\mathbf{E}$.

solution of the periodically forced difference equations. A general proof of this is given in [4].

3. ORIGIN OF THE MAGNETIC OFFSET

Let $e^{i\omega t}\tilde{\mathbf{E}}$ and $e^{i\omega t}\tilde{\mathbf{H}}$ denote the periodic solutions obtained by solving the periodically forced differential equations without the initial conditions. We shall assume that the solutions $\mathbf{E}$ and $\mathbf{H}$ of the initial value problem are such that for large times,

$$\mathbf{E}(\mathbf{x},t) \sim e^{i\omega t}\tilde{\mathbf{E}}(\mathbf{x}), \qquad \mathbf{H}(\mathbf{x},t) \sim e^{i\omega t}\tilde{\mathbf{H}}(\mathbf{x}) + \mathbf{H}^*(\mathbf{x}). \tag{7}$$

These assumptions reflect what is seen computationally.

Since $e^{i\omega t}\tilde{\mathbf{E}}$ and $e^{i\omega t}\tilde{\mathbf{H}}$ satisfy the same equations as $\mathbf{E}$ and $\mathbf{H}$ (excluding the initial conditions) we obtain by subtraction the following equations for $\mathbf{H}^*$:

$$\begin{aligned} \operatorname{div}\mathbf{H}^* &= 0 && (8)\\ \mathbf{curl}\,\mathbf{H}^* &= 0 && (9)\\ \frac{\partial \mathbf{H}^*}{\partial t} &= 0 && (10)\\ \mathbf{H}^* \times \mathbf{n}|_{\Gamma_o} &= 0. && (11) \end{aligned}$$

To obtain a boundary condition on the scatterer we integrate Faraday's law with respect to time, use the initial conditions and evaluate the normal components on Γ_s:

$$\mathbf{H}(\mathbf{x})\cdot\mathbf{n} = \mathbf{H}_0(\mathbf{x})\cdot\mathbf{n} - \frac{1}{\mu}\int_0^t \mathbf{curl}\,\mathbf{E}(\mathbf{x},\tau)\cdot\mathbf{n}\,d\tau \qquad \text{on } \Gamma_s.$$

Since $\mathbf{curl}\,\mathbf{E}\cdot\mathbf{n}$ on Γ_s is the tangential derivative of $\mathbf{E}$ along the boundary, it is completely determined by the boundary condition. So

$$\mathbf{H}(\mathbf{x})\cdot\mathbf{n} \;=\; \mathbf{H}_0(\mathbf{x})\cdot\mathbf{n} + \frac{1}{\mu}\int_0^t \mathbf{curl}\,\mathbf{E}_i(\mathbf{x},\tau)\cdot\mathbf{n}\,d\tau$$

$$= \left(\mathbf{H}_0(\mathbf{x})\cdot\mathbf{n} - \frac{1}{i\omega\mu}\mathbf{curl}\,\widetilde{\mathbf{E}}_i(\mathbf{x})\cdot\mathbf{n}\right) + \frac{e^{i\omega t}}{i\omega\mu}\mathbf{curl}\,\widetilde{\mathbf{E}}_i(\mathbf{x})\cdot\mathbf{n} \qquad \text{on } \Gamma_s.$$

In the above expression it is only the second term which has the required periodic behavior and it follows that the first term, which is stationary, must correspond to the normal boundary condition for $\mathbf{H}^*$. Thus we are led to

$$\mathbf{H}^*\cdot\mathbf{n}|_{\Gamma_s} = (\mathbf{H}_0\cdot\mathbf{n} - \frac{1}{i\omega\mu}\mathbf{curl}\,\widetilde{\mathbf{E}}_i\cdot\mathbf{n})|_{\Gamma_s}. \tag{12}$$

To interpret this boundary condition, assume that the incident magnetic field is also of the form $e^{i\omega t}\widetilde{\mathbf{H}}_i(\mathbf{x})$ such that Maxwell's equations are satisfied. In that case Faraday's law gives

$$e^{i\omega t}\widetilde{\mathbf{H}}_i(\mathbf{x}) = \frac{1}{i\omega\mu}e^{i\omega t}\mathbf{curl}\,\widetilde{\mathbf{E}}_i$$

and evaluating this at $t = 0$ and using it to replace the second term in the boundary condition it follows that $\mathbf{H}^*\cdot\mathbf{n}$ is the normal component of the *total* magnetic field at $t = 0$. Since $\mathbf{B}\cdot\mathbf{n}$ must be continuous across Γ_s it follows that there is a magnetic field inside the scatterer if the right side of (12) is nonzero. In addition this field is stationary since $\mathbf{E}$ is zero inside a perfect conductor, and we may attribute it to a steady current flowing unhindered in the conductor. It is this current which produces the magnetic offset.

4. AVOIDING THE MAGNETIC OFFSET

In this section we will discuss four different possibilities for obtaining the correct magnetic field $e^{i\omega t}\widetilde{\mathbf{H}}(\mathbf{x})$. The first approach is a simple postprocessing technique which does not use the results of the previous sections except for the assumptions (7). The other three approaches do rely on the equations obtained in the previous sections.

Method 1: Postprocessing. The postprocessing approach consists simply of fitting a function of the form $A + Be^{i\omega t}$ to the computed $\mathbf{H}$ at each mesh point, and then discarding the stationary part A. A decision has to be made about when to sample $\mathbf{H}$. This should be at reasonably spaced times after the solution is believed to have become adequately periodic (3–6 periods is often sufficient).

To illustrate the stationary part we took a square scatterer as before and illuminated it from the (1,0) direction with a field $\mathbf{E}_i(\mathbf{x},t) = 1000e^{i(\omega t - \mathbf{k}\cdot\mathbf{x})}$. The problem was solved (for the imaginary part of the solution) by the method mentioned above in section 2, starting from zero initial conditions. We calculated (the imaginary part of) the stationary part by sampling the values of $\mathbf{H}$ after m, $m - \frac{T}{4}$ and $m - \frac{T}{2}$ timesteps, where T is the period of the incident field in timesteps, for $m = 500$ and $m = 1000$ (about 4 and 8 periods). The values of the stationary parts of the x- and y-components of $\mathbf{H}$ on lines $y = \frac{20.5}{20\pi}$ and $y = \frac{1}{\pi}$, respectively, are shown in figures 3 and 4. Also shown are the theoretically predicted values of the stationary field $\mathbf{H}^*$ (the approximate solution of (8)–(12)). We see that the values of

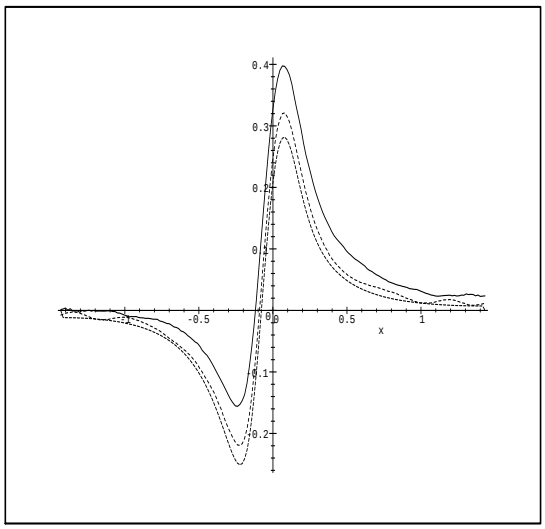

Figure 3: The stationary part of $\mathbf{H}_x$.

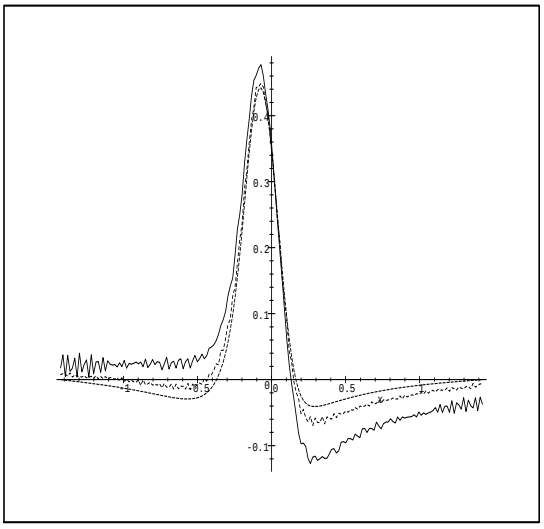

Figure 4: The stationary part of $\mathbf{H}_y$.

Postprocessing method (zero initial data)
500 timesteps — solid line, 1000 timesteps — dashed line, $\mathbf{H}^*$ — dotted line.

$\mathbf{H}^*$ are quite near to the stationary parts of $\mathbf{H}$, especially for longer time. The stationary part is relatively large compared to the amplitude of $\mathbf{H}$, which is near one for most of Ω.

Method 2: Solving the div-curl system. The second approach to elimination of the magnetic offset is based on the observation from (12) that if the initial condition for $\mathbf{H}$ satisfies $\mathbf{H}_0 \cdot \mathbf{n} = \frac{1}{i\omega\mu}\mathbf{curl}\ \widetilde{\mathbf{E}}_i \cdot \mathbf{n}$ on Γ_s, then the div-curl system for $\mathbf{H}^*$ will have only the zero solution. One way to choose a suitable $\mathbf{H}_0$ is as a solution of the equations

$$\mathbf{curl}\ \mathbf{H}_0 = 0 \tag{13}$$

$$\mathrm{div}\ \mathbf{H}_0 = 0 \tag{14}$$

$$\mathbf{H}_0 \cdot \mathbf{n} = \frac{1}{i\omega\mu}\mathbf{curl}\ \widetilde{\mathbf{E}}_i \cdot \mathbf{n} \quad \text{on } \Gamma_s \tag{15}$$

$$\mathbf{H}_0 \times \mathbf{n} = 0 \quad \text{on } \Gamma_o. \tag{16}$$

To illustrate this we solved Maxwell equations with the initial conditions $\mathbf{E}_0 = 0$ and $\mathbf{H}_0$ being the solution of (14)–(16). Then we calculated the stationary part as above. The results (the values of the stationary parts of the x- and y-components of $\mathbf{H}$ on lines $y = \frac{20.5}{20\pi}$ and $y = \frac{1}{\pi}$, as before) are shown in Figures 5 and 6.

One can see that the stationary part is several times smaller than in the postprocessing method; in fact it is probably caused by the discretization error in time. However, even though there is a natural way to formulate the div-curl system in the FDTD framework,

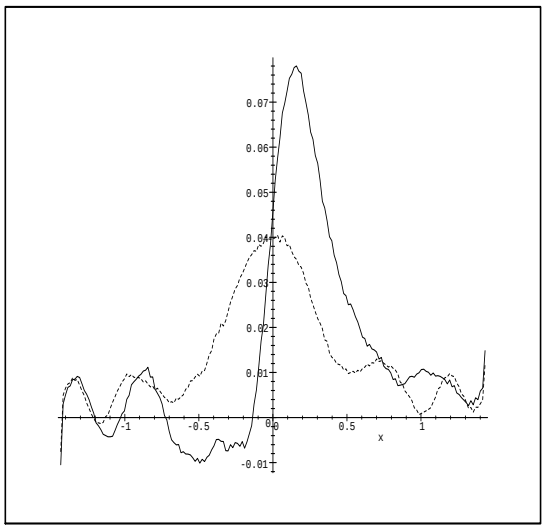

Figure 5: The stationary part of $\mathbf{H}_x$.

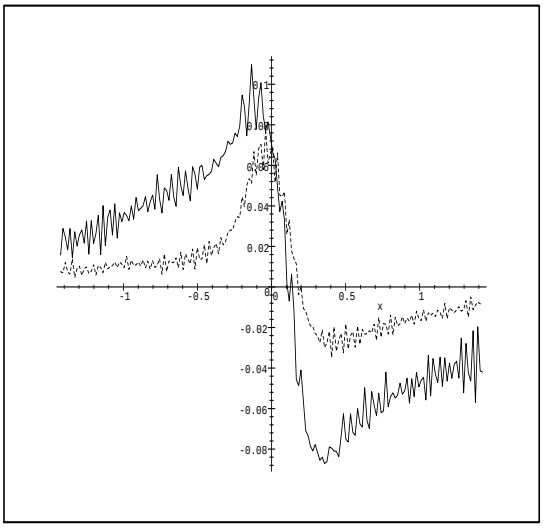

Figure 6: The stationary part of $\mathbf{H}_y$.

$\mathbf{H}_0$ is a solution of the div-curl problem (14)–(16).
500 timesteps — solid line, 1000 timesteps — dashed line

solving it can be quite expensive. Also, up to round-off error the solution is similar to that of the postprocessing method after discarding the stationary part. So it seems that this method is not worth while.

Method 3: Extension of $\widetilde{\mathbf{E}}_i$. Another way to satisfy the condition $\mathbf{H}_0 \cdot \mathbf{n} = \dfrac{1}{i\omega\mu}\mathbf{curl}\,\widetilde{\mathbf{E}}_i \cdot \mathbf{n}$ on Γ_s is to use the initial conditions

$$\mathbf{E}_0(\mathbf{x}) = -\phi(\mathbf{x})\widetilde{\mathbf{E}}_i(\mathbf{x}), \quad \mathbf{H}_0(\mathbf{x}) = \frac{1}{i\omega\mu}\mathbf{curl}\,(\phi(\mathbf{x})\widetilde{\mathbf{E}}_i(\mathbf{x})), \tag{17}$$

where ϕ is a smooth real-valued function such that $\phi \equiv 1$ in a neighborhood of Γ_s, and $\phi \equiv 0$ in a neighborhood of Γ_o. A possible advantage of this scheme is that since the initial values and the boundary data match at $t = 0$, the solution should be smoother in time for small times. We would then expect that discretizations should have a better rate of convergence as the mesh size approaches zero.

We used for ϕ a product of continuously differentiable cubic splines in x and in y. The resulting "stationary field" is shown on Figures 7 and 8. We see that it is much smaller than in the previous case, especially for longer time (40-80 times smaller after 1000 timesteps).

Method 4: Modified incident field. This method consists of giving zero initial data and making an adjustment to the incident field. It is possible to change this field for a small interval of time so that the spurious field will be zero. One possibility is to define the

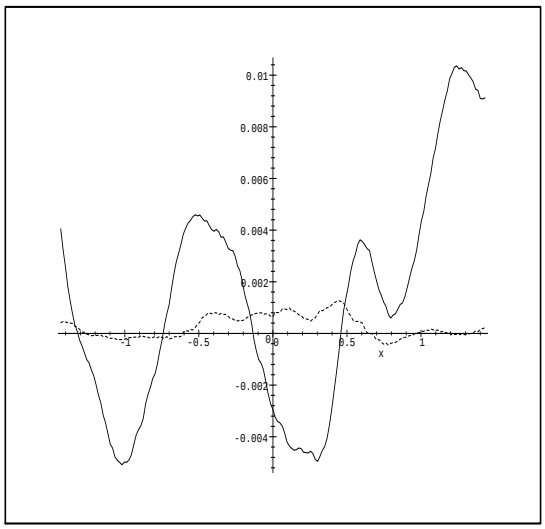

Figure 7: The stationary part of $\mathbf{H}_x$.

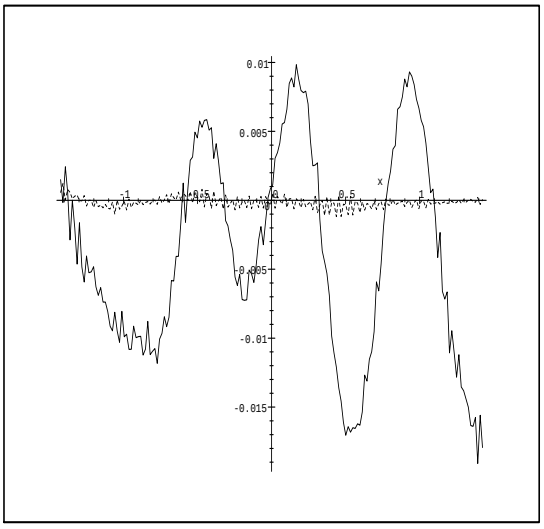

Figure 8: The stationary part of $\mathbf{H}_y$.

The smooth initial data (17).
500 timesteps — solid line, 1000 timesteps — dashed line

incident field to be

$$\mathbf{E}_i(\mathbf{x},t) = \begin{cases} \dfrac{\omega t}{2\pi} e^{i\omega t}\widetilde{\mathbf{E}}_i(\mathbf{x}), & 0 \le t \le \dfrac{2\pi}{\omega}, \\ e^{i\omega t}\widetilde{\mathbf{E}}_i(\mathbf{x}), & t > \dfrac{2\pi}{\omega}. \end{cases} \tag{18}$$

Then at time $t_0 = \frac{2\pi}{\omega}$, on Γ_s we have

$$\mathbf{H}(\mathbf{x},t_0)\cdot\mathbf{n} = \frac{1}{\mu}\int_0^{t_0} \frac{t}{t_0} e^{i\omega t} dt\, \mathbf{curl}\ \widetilde{\mathbf{E}}_i(\mathbf{x})\cdot\mathbf{n} = \frac{1}{i\omega\mu} e^{i\omega t_0}\mathbf{curl}\ \widetilde{\mathbf{E}}_i(\mathbf{x})\cdot\mathbf{n}, \tag{19}$$

so that $\mathbf{H}(\mathbf{x},t_0)$ satisfies the correct condition at time $t_0 = \frac{2\pi}{\omega}$. Again the initial and the boundary conditions match, so the solution is smoother. Since the incident field reaches the correct value after the first period, the additional work required is roughly equal to solving the equations during one period.

The results are shown in Figures 9 and 10.

For an incident field in the form $e^{i(\omega t - \mathbf{k}\cdot\mathbf{x})}$ it might be preferable to adjust the field as follows:

$$\mathbf{E}_i(\mathbf{x},t) = \begin{cases} 0, & \omega t \le \mathbf{k}\cdot\mathbf{x}, \\ \dfrac{\omega t - \mathbf{k}\cdot\mathbf{x}}{2\pi} e^{i(\omega t - \mathbf{k}\cdot\mathbf{x})}, & 0 < \omega t - \mathbf{k}\cdot\mathbf{x} \le 2\pi, \\ e^{i(\omega t - \mathbf{k}\cdot\mathbf{x})}, & 2\pi < \omega t - \mathbf{k}\cdot\mathbf{x}. \end{cases} \tag{20}$$

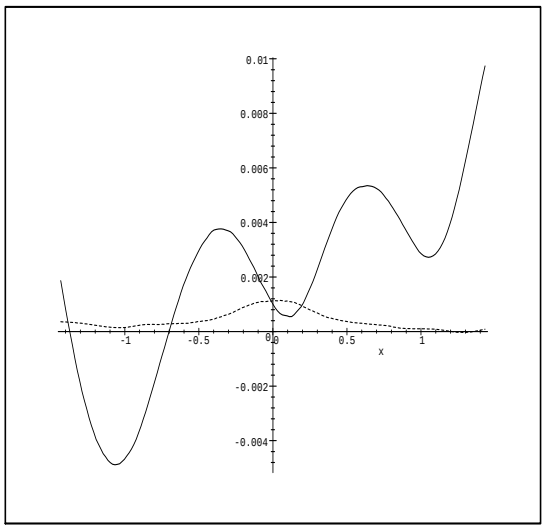

Figure 9: The stationary part of $\mathbf{H}_x$.

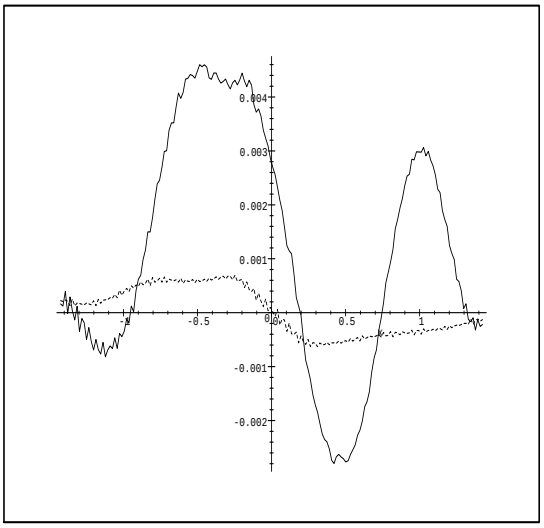

Figure 10: The stationary part of $\mathbf{H}_y$.

Continuous adjustment of the incident field, given by (18).
500 timesteps — solid line, 1000 timesteps — dashed line

Again at time t_0 large enough so that the incident field has reached the correct value on all Γ_s, we get that $\mathbf{H}(\mathbf{x}, t_0)$ satisfies the condition necessary to make the spurious field vanish. This adjustment makes the imaginary part of $\mathbf{E}_i$ continuously differentiable, so we should get even better convergence when solving for the imaginary part only. The results are shown in Figures 11 and 12. (We used $m = 600$ instead of $m = 500$, because after 4 periods the adjusted incident field has barely reached its correct value near the outer boundary.) Note that the stationary parts are the smallest compared with the other methods.

To compare the smoothness of the solutions obtained by the different methods we present here the time history of $\mathbf{H}_x$ at the point $(-\frac{1}{\pi}, \frac{1}{40\pi})$. This point, as any point near the x-axis, is special in the sense that the amplitude of $\mathbf{H}_x$ is very small, so effects of nonsmoothness stand out more clearly. Figure 13 shows the solutions with zero initial data (method 1) and in the case of "correct" smooth initial data (17) (method 3). The graph of the solution obtained by first solving the div-curl system (method 2) looks the same as of the solution obtained by method 1, only shifted by a constant (the size of the shift is determined by the value of the solution of the div-curl problem at given point), so we chose not to present it here. The solutions exhibit very large oscillations in the beginning. They correspond to a large error in approximating the discontinuous wavefront. As the front moves away, the solution becames smoother. Then the oscillations reappear approximately at the time when the (reflected) wavefront arrives back from the corners of the artificial boundary (the reflections from the smooth part of the boundary are probably too small to be seen). Figure

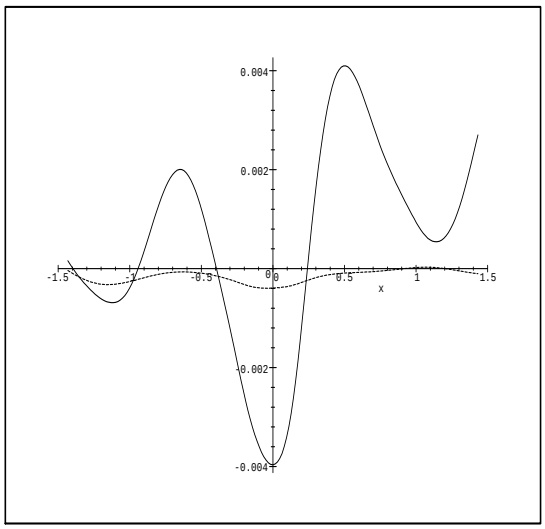

Figure 11: The stationary part of $\mathbf{H}_x$.

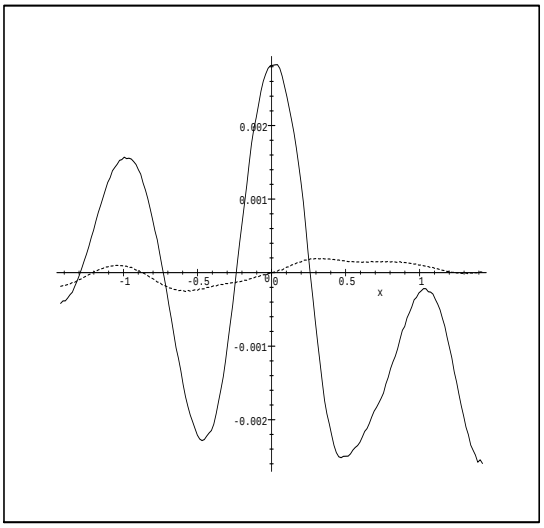

Figure 12: The stationary part of $\mathbf{H}_y$.

Smooth adjustment of the incident field, given by (20).
600 timesteps — solid line, 1000 timesteps — dashed line

14 shows the solutions with zero initial data and altered boundary conditions (method 4, boundary conditions (18) and (20)). We see that the solution looks much smoother than the solutions obtained with the other methods, so one might expect to have smaller discretization error than in the other cases.

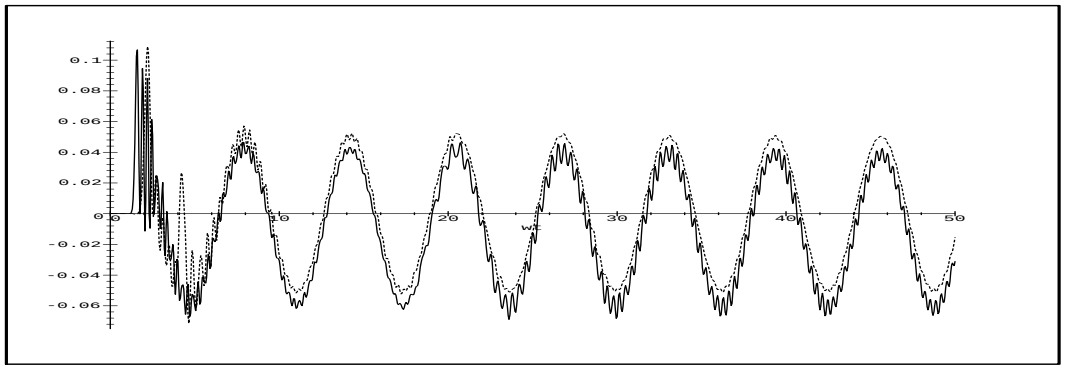

Figure 13: The time history of $\mathbf{H}_x$ at the point $(-\frac{1}{\pi}, \frac{1}{40\pi})$ in the case of zero initial data (solid line) and the smooth initial data (17) (dashed line).

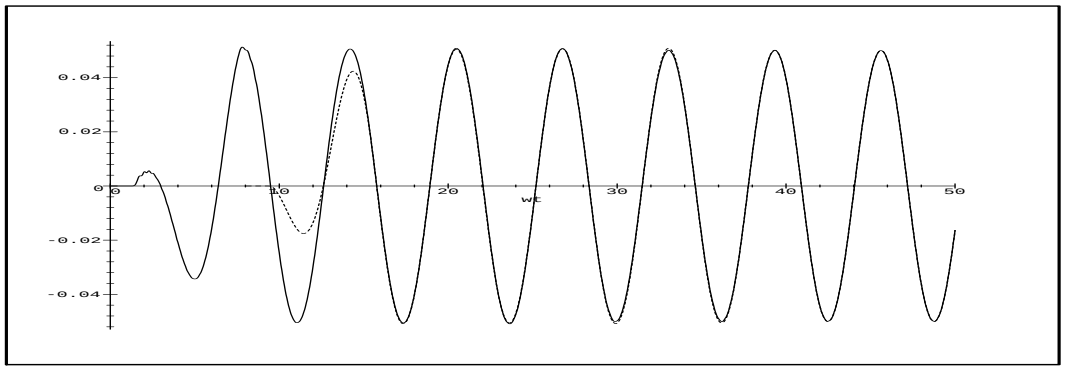

Figure 14: The time history of $\mathbf{H}_x$ at the point $(-\frac{1}{\pi}, \frac{1}{40\pi})$ in the case of continuous adjustment of the boundary conditions, given by (18) (solid line), and in the case of smooth adjustment (20) (dashed line), both with zero initial data.

5. OTHER PROBLEMS

Consider the transverse electric problem: in Ω,

$$\begin{aligned} \epsilon \frac{\partial \mathbf{E}}{\partial t} &= \mathbf{curl}\, \mathbf{H} \\ \mu \frac{\partial \mathbf{H}}{\partial t} &= -\mathbf{curl}\, \mathbf{E} \\ \mathrm{div}\, \mathbf{E} &= 0 \end{aligned}$$

with boundary conditions

$$\begin{aligned} \mathbf{E} \times \mathbf{n} &= -\mathbf{E}_i \times \mathbf{n} \qquad \text{on } \Gamma_s \\ \mathbf{E} \times \mathbf{n} + c\mu \mathbf{H} &= 0 \qquad \text{on } \Gamma_o \end{aligned}$$

and initial conditions

$$\mathbf{E}(\mathbf{x},0) = \mathbf{E}_0(\mathbf{x}), \qquad \mathbf{H}(\mathbf{x},0) = \mathbf{H}_0(\mathbf{x}).$$

In this case there is an *electric* offset. The magnetic offset is zero because $\mathbf{H}\cdot\mathbf{n} = 0$ on Γ_s holds automatically.

Assuming that for large times

$$\mathbf{E}(\mathbf{x},t) \sim e^{i\omega t}\widetilde{\mathbf{E}}(\mathbf{x}) + \mathbf{E}^*(\mathbf{x}), \quad \mathbf{H}(\mathbf{x},t) \sim e^{i\omega t}\widetilde{\mathbf{H}}(\mathbf{x}),$$

we obtain as before by subtraction the following equations for $\mathbf{E}^*$:

$$\begin{aligned} \frac{\partial \mathbf{E}^*}{\partial t} &= 0 \\ \mathbf{curl}\ \mathbf{E}^* &= 0 \\ \mathrm{div}\ \mathbf{E}^* &= 0 \\ \mathbf{E}^*\times\mathbf{n} &= 0 \quad \text{on } \Gamma_o \text{ and on } \Gamma_s \end{aligned}$$

A system such as this is determined up to a one parameter family of solutions. In this case the parameter is the total surface charge on the body. This quantity should be zero to avoid a spurious addition to the electric field. It is computed as follows:

$$\int_{\Gamma_s} \mathbf{E}\cdot\mathbf{n} = \int_{\Gamma_s} \mathbf{E}_0\cdot\mathbf{n} + \frac{1}{\epsilon}\int_0^t \int_{\Gamma_s} \mathbf{curl}\ \mathbf{H}\cdot\mathbf{n} = \int_{\Gamma_s} \mathbf{E}_0\cdot\mathbf{n}.$$

It follows that the total charge is constant in time and it is this charge, determined by the initial condition, which is responsible for the electric offset field. The simplest way to eliminate the electric offset is to put $\mathbf{E}_0 \equiv 0$. The system above, supplemented with this condition of zero surface charge then has only the zero solution.

For the three dimensional case the calculations above remain valid so both the electric and magnetic fields may have spurious components. Our equations for $\mathbf{E}^*$ and $\mathbf{H}^*$ continue to hold and so should the remedies although we have not checked that explicitly.

It has not been possible to completely rule out the possibility of additional (possibly time dependent) spurious fields in three dimensions although we do not expect that such fields exist.

6. MATHEMATICAL COMMENTS

We have made a number of assumptions in order to obtain the equations for the offset fields. We wish to mention the major assumptions here.

First there is the question of whether the equations (1)–(6) admit a periodic solution. This is equivalent to the question of existence for Helmholtz equation in a bounded domain with the appropriate boundary conditions. We have assumed here that periodic solutions exist.

A second assumption is that the solutions of the initial value problems with periodic boundary conditions approach to a limiting state as $t \to \infty$. While this is certainly expected for reasonably shaped scatterers, it should be proved in a precise treatment.

The third assumption is the one we justified by appeal to computational experiments, which is that in the transverse magnetic (electric) case the electric (magnetic) field has no offset so that $\mathbf{E}(\mathbf{x},t) - e^{i\omega t}\widetilde{\mathbf{E}}(\mathbf{x}) \to 0$ as $t \to \infty$ ($\mathbf{H}(\mathbf{x},t) - e^{i\omega t}\widetilde{\mathbf{H}}(\mathbf{x}) \to 0$) as $t \to \infty$. Since in the transverse magnetic (electric) problem $\mathbf{E}$ ($\mathbf{H}$) is one-dimensional, this is really a question of the asymptotic behavior of the wave equation with periodic Dirichlet (Neumann) condition on the inner boundary and the absorbing boundary condition on the outer boundary. This has been known for a while. For three dimensions the question is more delicate, because the equations are coupled by divergence conditions, and also because both the electric and the magnetic field may have spurious components.

In our paper [4], which is a companion to this one, we provide a rigorous statement of these assumptions and the appropriate results are proved correct for the two dimensional problems.

7. CONCLUSIONS

We have shown the origin of the spurious magnetic and electric offset fields which are encountered when time marching Maxwell equations for periodic solutions. Based on the equations governing these fields several remedies were discussed. We found that the best remedy is to modify the incident field, gradually allowing it to reach its desired form in the way specified in section 4. This technique reliably reduces the magnetic offset to a negligible size and avoids the need for postprocessing of the results of the computation.

REFERENCES

[1] A.Taflove. Computational Electrodynamics. The Finite Difference Time Domain Method. Artech House 1995.

[2] A. Taflove and K. R. Umashankar. Review of numerical modeling of electromagnetic wave scattering and radar cross section. Proc. IEEE,77, 5, p682, 1989.

[3] C. M. Furse, S. P. Mathur and O. P. Gandhi. Improvements to the finite–difference time–domain method for calculating the radar cross section of a perfectly conducting target. IEEE Trans. Microwave Theory and Techniques, 38, 7, p919, 1990.

[4] U. Kangro and R. A. Nicolaides. Asymptotic Behavior of Solutions of Periodic Scattering Problems in Electromagnetics. (To appear in SIAM Journal of Mathematical Analysis).